Intergenic accumulation of RNAPII maintains the potential for swift transcriptional restart upon release from quiescence

Manuela Baquero Pérez, Gertjan Laenen, Isabelle Loïodice, et al.

Genome Res. published online August 12, 2025
Access the most recent version at doi:10.1101/gr.279874.124

Intergenic accumulation of RNAPII maintains the potential for swift transcriptional re-start upon release from quiescence

Baquero Pérez, Manuela [1]

Laenen, Gertjan [1] **

Loïodice, Isabelle [1] **

Mickaël Garnier [1]

Szachnowski, Ugo [2]

Morillon, Antonin [2]

Ruault, Myriam [1]

Taddei, Angela [1]

Affiliations

[1] Institut Curie, Université PSL, Sorbonne University, CNRS, UMR3664 Nuclear Dynamics, Paris, France

[2] Institut Curie, Université PSL, Sorbonne University, CNRS, UMR3244 DIG-Cancer, Paris, France

** Equally contributing authors

Running title: Transcription dynamics in and out quiescence

Key words: Quiescence, return to growth, RNA Pol II, nuclear organization, Single-Cell RNA-Seq

Data accession numbers: E-MTAB-14337 (ChIP-seq); E-MTAB-14980 (scRNA-seq); E-MTAB-14983 (RNAseq)

ABSTRACT (224/250 words)

Quiescent cells (Q) are seemingly inactive, developmentally arrested cells, whose universal characteristic is the ability to promptly re-enter the cell cycle upon sensing of external cues. Q cells are responsive to the environment and flexible enough to adapt to available resources. In budding yeast, quiescent nuclear features are drastically distinct from those observed in nutrient replete conditions: the nuclear volume is reduced, the telomeres relocate from the nuclear periphery to the center of the nucleus into a hypercluster, chromatin is found in a compacted, hypo-acetylated state, and transcription is globally shutdown. Yet, Q cells can re-start transcription within minutes of re-feeding. Here, we follow the global decrease of transcription in sorted, developing Q populations, and its reactivation upon release. We find that transcription and telomere clustering dynamics in and out of quiescence are independent events. We report a genome-wide re-distribution of the transcription machinery as cells progress into quiescence. Although most genes are shut down, 3% of coding genes remain active. Furthermore, RNAPII accumulates at one third of gene promoters. The corresponding genes are highly enriched among those showing a high level of transcription and high frequency of expression in individual cells, shortly after cells are refed, as monitored by single-cell RNASeq. Our results point toward a role for quiescent-specific RNAPII distribution to ensure a rapid and robust transcriptional response upon return to growth.

INTRODUCTION

Eukaryotic genome organization is dynamic, varying across cell types and conditions, both functionally and spatially. These adaptations can be subtle, like individual gene repositioning upon activation (Abruzzi et al. 2006; Brickner and Walter 2004; Casolari et al. 2004; Taddei et al. 2006), or drastic, such as whole-genome reorganizations during development or metabolic transitions (Guidi et al. 2015; Bourbousse et al. 2020; Feodorova et al. 2020). In this study, we explore the transitions in and out of quiescence in budding yeast, aiming to understand how the genome adapts to environmental changes.

S. cerevisiae undergoes a number ofmetabolic transitions, favoring glucose fermentation in rich medium and activating alternative metabolic pathways and stress-response genes as glucose depletes. When glucose runs out, cells enter the diauxic shift, transitioning to ethanol metabolism, with a growth arrest and a twofold decrease in transcription (DeRisi 1997; Gasch and Werner-Washburne 2002; McKnight et al. 2015; Miles et al. 2013; Young et al. 2017). Cells will then progressively exhaust their medium, reaching stationary phase within 3 to 7 days (Gray et al. 2004; Miles et al. 2021; Opalek et al. 2023; Werner-Washburne et al. 1996). From the early post-diauxic shift phase, two populations of cells develop, with highly dense quiescent (Q) cells that can be separated from lowly dense cells non quiescent (NQ) along a density gradient (Allen et al. 2006). Q cells exhibit remarkable stress resistance and longevity, compared to the rest of the population that is heterogeneous in terms of viability (Allen et al. 2006; Aragon et al. 2008; Davidson et al. 2011). Transcriptome analysis shows a 2- to 30-fold reduction in transcription in quiescent cells compared to cycling cells (McKnight et al. 2015;

Young et al. 2017). Yet, upon nutrient restoration, a robust and swift transcriptional re-ignition is observed within minutes.

The RSC remodeling complex was proposed to play a crucial role in this rapid re-ignition of transcription upon nutrient addition (Cucinotta et al. 2021). However, the extent to which the transcription machinery is associated with the quiescent genome is still debated, with early studies indicating poised RNAPII upstream of genes (Radonjic et al. 2005) and recent studies reporting either a different distribution, towards the 3' end of coding sequences (Young et al. 2017), or no association of RNAPII to intergenic regions (Cucinotta et al. 2021; Young et al. 2017).

Changes in transcriptional activity are accompanied by a global change in chromatin and nuclear organization in Q cells. The quiescent genome is compacted (Schäfer et al. 2008; Swygert et al. 2019, 2021), and globally de-acetylated at promoters targeted by Rpd3 (McKnight et al. 2015). Telomeres in quiescent cells hypercluster in a *SIR3*-dependent manner (Guidi et al. 2015). Although it has been suggested that condensin-dependent compaction plays a role in transcriptional shutdown (Swygert et al. 2019), the interplay between hyperclustering and transcriptional activity has not been explored.

Here we aim to shed light on the state of transcription upon quiescence entry and return to growth, in relation to spatial constraints and rearrangements in the nucleus.

RESULTS

Transcriptional shutdown during quiescence entry occurs independently of telomere hypercluster formation

We sought to dissect the process of transcriptional shutdown as cells enter quiescence and understand its functional relationship with telomere hypercluster

formation. We mapped the genome-wide transcription machinery occupancy by quantitative chromatin-immunoprecipitation of the Rpb3 subunit fused to a FLAG tag (methods). In parallel, using the same strain, we followed the subnuclear distribution of the telomere-bound protein Rap1 fused to GFP. Cells from post-diauxic shift cultures onwards were purified using a density-based gradient, as described in (Allen et al. 2006), to mainly retrieve the developing Q population. We followed entry into quiescence in two nutrient depletion conditions (Fig. 1A). (i) We grew cells in glucose-rich medium and examined samples at different stages as the population grows into stationary phase (SP): cells growing exponentially by fermenting glucose (Log), undergoing diauxic shift (DS), and purified highly dense (HD) cells from post-diauxic cultures at 1 (day 1-HD), 2 (day 2-HD), and 6 days-HD (Q) after inoculation. (ii) Alternatively, we induced quiescence by *abrupt starvation* of post-diauxic shift cells for 24 hours (Q-like).

As previously described (Guidi et al. 2015), clustering of telomeres changes as cells transition from exponential growth by fermenting glucose (Log), through slowed-down growth in the post-diauxic shift phase (PDS, day 1 HD). The proportion of nuclei with more than 3 clusters is reduced, and foci become brighter. Hyperclusters (Guidi et al. 2015), defined here as clusters that are 4 times brighter than the median of clusters in Log phase, increase in proportion from day 2 onwards (Fig 1B).

Total RNAPII levels show little variation upon growth into stationary phase and quiescence entry (Jona et al. 2000; Radonjic et al. 2005; Young et al. 2017). In contrast, genome-wide counts of spike-in calibrated RNAPII ChIP-seq show varying levels of the transcription machinery associated with the genome in these kinetics (Fig. 1B, bottom). First, RNAPII genome association decreases 2 and 1.4-fold respectively in diauxic-shift (DS) and early respiration (day 1 HD) samples relative to

exponential phase (Log). All samples after 2 days of growth show more than a 3-fold decrease relative to Log. We previously showed that both Q (6 days of nutrient exhaustion) and Q-like (abrupt starvation) cells display telomere hyperclusters (Guidi et al. 2015). Here we show that these two stages are associated with very low Rpb3-FLAG occupancy genome-wide. Furthermore, while decrease of RNAPII occupancy and increase of telomere hypercluster follow a similar trend over the kinetics of quiescence entry, the former precedes the latter, as minimal RNAPII occupancy (6.2-fold decrease relative to Log) is observed after 2 days of growth and telomere hyperclustering keeps increasing up to 6 days.

To test whether hypercluster formation is required for transcriptional shutdown, we examined RNAPII binding in a *sir3*Δ mutant, defective for hypercluster formation, but able to form highly dense, small cells, morphologically similar to WT (Guidi et al. 2015) and Fig. 1C). To avoid pseudo-diploidy effects owing from the derepression of cryptic mating type loci in *sir3*Δ strains (Galitski et al. 1999), we worked in an *hml*Δ background. As expected, RNAPII binding is higher at subtelomeric loci in *sir3*Δ cycling cells (Log) (Supplemental Fig. S1A). Yet, Rpb3-FLAG ChIP-seq samples in *sir3*Δ background highly correlate with WT (Fig. 1C; Supplemental Fig. S1B) in Log and Q samples, including at 297 genes with significant Rpb3-FLAG binding in quiescent chromatin (Supplemental Fig. S1C), demonstrating that shutdown of transcription does not depend on telomere hyperclustering. Therefore, during quiescence entry, transcriptional shutdown precedes and occurs independently of telomere hyperclustering.

Dismantling of telomere hypercluster follows but is independent of transcriptional activation upon return to growth.

We next asked when telomere hyperclusters dismantle upon return to growth and whether it depends on transcriptional activation that occurs within 3-10 minutes after refeeding (Cucinotta et al. 2021; Martinez et al. 2004; Radonjic et al. 2005). We followed Rap1-GFP in released quiescent cells and found hyperclusters disassembling within 15-30 minutes, one hour before S-phase starts as monitored by bud emergence (Fig 2A). De-clustering is particularly apparent in the decrease in brightness of clusters, which reach intensities comparable to those found in cycling cells after 30 minutes of release in glucose (Fig 2B; Supplemental Fig S2A). Thus, hypercluster dismantling occurs swiftly but it only comes after re-ignition of transcription.

To test whether transcriptional activation could be the cause of telomere hypercluster dismantling, we followed telomere clusters after releasing the thermosensitive *rpb1-1* strain at restrictive temperature. RNA-seq confirmed a severe defect of transcriptional activation (Supplementary Fig. S2B) and a close to wild-type kinetic of declustering in these conditions. Similar results were observed in cells pre-treated with the RNAPII inhibitor phenanthroline (Supplemental Fig. S2C). In contrast, quiescent cells treated with thiolutin did not dismantle their telomere hyperclusters, confirming the complex effect of this drug (Eshleman et al. 2020; Qiu et al. 2024; Lauinger et al. 2017). We thus conclude that hypercluster dismantling upon quiescence exit is largely independent of RNAPII activity.

Scant transcription of poorly characterized genes remains in the quiescent population

We examined the genome-wide distribution of RNAPII through our spike-in calibrated Rpb3-FLAG mappings, which shows no bias in distribution along the chromosome arms, except for a two-fold increase of counts of Rpb3-FLAG at the

rDNA locus observed both in WT and *sir3*Δ cells (Supplemental Fig. S3A,B) that is accompanied by a decrease in RNAPI occupancy (Supplemental Fig. S3C), consistent with a smaller nucleolus and reduced protein synthesis (Guidi et al. 2015; Fuge et al. 1994; Laporte et al. 2013). These observations suggest a competitive binding of RNAPII and RNAPI as was previously proposed (Cioci et al. 2003).

As cells progress into quiescence, Rpb3-FLAG signal is depleted over genes and intergenes alike (Supplemental Fig. S3D). To address the extent of shutdown, we examined RNAPII annotations. Since non-coding annotations do not particularly show a quiescence-specific increase in Rpb3-FLAG binding (Supplemental Fig. S3E), we focused our analyses on the transcription of protein-coding genes. Importantly, Rpb3-FLAG presence over gene bodies correlates very well with previous mappings of untagged Rpb3 (pearson and spearman R=0.8) and of the Ser2 phosphorylation of the C-terminal domain (CTD) of Rpb1 (pearson R= 0.87, spearman R=0.85) in quiescence (Swygert et al. 2019), associated with its elongating form (Fig. 3A). Based on the presence or absence of Rpb3-FLAG and newly synthesized transcripts (4tU-seq) (Cucinotta et al. 2021) (methods) we define 4 classes of genes.

Amongst the 297 genes that are bound by RNAPII in Q, more than half show newly synthesized transcripts in Q cells (class I, 161 genes), while the rest, which are shorter (Supplemental Fig. S3F), do not (class II, 136 genes). Of note *sir3*Δ strain shows similar RNAPII binding profile at these genes (Supplemental Fig. S1C).

One-third of all protein coding genes show detectable transcripts but Rpb3-FLAG counts below the threshold (class III, 1916), while about half do not meet the threshold for Rpb3-FLAG or 4tU-seq counts (class IV, 3602). Class III genes show on average less recently synthesized transcripts than class I and more RNAPII than

class IV (Supplemental Fig. S3F), thus showing consistency between 4tU and RNAPII detection. The presence of 4tU signal at these genes with no detectable RNAPII in their gene body could reflect the difference in sensitivity between ChIP and 4tU detection.

Class I and II show comparable levels of Rpb3-FLAG binding but differ in 4tU-seq counts. Class II genes being particularly small (Supplemental Fig. S3F), size bias and/or reduced stability of transcripts might account for less efficient capture of 4tU-seq reads assigned to these genes. In addition, differences between 4tU incorporation and RNAPII binding could stem from small variations between growth conditions. While both class I and class II are enriched in uncharacterized ORFs, class II genes are also enriched in dubious ORFs (Supplemental Fig. S3G). Thus, class II genes show overall less evidence for *bona fide* transcription in quiescent cells than class I genes. Curiously, 55/136 class II genes do not show RNAPII binding in fermentation or respiration. In contrast, almost all class I genes were bound by RNAPII during growth: most during all growth phases (112), some (49) specifically after the diauxic shift (Supplemental Fig. S3H). Only few class I genes are annotated as verified ORFs (62 genes) and show an enrichment for catabolic processes and carboxylic acid transport (Supplemental Fig. S3G). Such little functional enrichment is consistent with class I genes being significantly enriched in uncharacterized ORFs (Supplemental Fig. S3G), in agreement with the scant characterization of quiescence. Only two verified ORFs, with little functional characterization, *RTS2* and *BSC4*, are bound exclusively in Q cells (Supplemental Fig. S3H).

Single cell RNA-seq confirms active transcription in Q cells.

Density gradients allow to enrich for the highly-dense population, also referred to as quiescent (Q)(Allen et al. 2006). To rule out that class I transcripts resulted from transcription in leftover low-density cells, or a subpopulation of Q cells, we examined the transcriptome of the population at the single-cell level, after adapting the 10× Genomics SC3' encapsulation protocol to quiescent cells ((Jariani et al. 2020; Vermeersch et al. 2022), methods). The correlation between pseudo-bulk scRNA-seq and 4tU-seq counts (Pearson R=0.6, Spearman's R=0.64), indicates that single cell RNA seq in quiescent cells detects mainly recently synthesized transcripts. This is in good agreement with the reported difficulty to extract stored mRNAs in quiescent cells (Aragon et al. 2006). UMAP dimensionality reduction of single-cell RNA-seq data revealed that our gradient-sorted population at 6 days of medium exhaustion show a bilobate structure (Fig. 3B). Nevertheless, class I transcripts are well-represented throughout both subpopulations (Fig. 3B), independently of read counts (Supplemental Fig. S3I). Indeed, these 161 genes make up one-third (35.6 %) of the transcriptome of the average cell (Supplemental Fig. S3J). Our single-cell analysis thus reveals a widespread transcription of 3% of protein-coding genes for the Q population.

Of note, seven class I genes are detected in more than 80% of the cells and collectively make up 18.8% of the average transcriptome, amongst which is *GRE1,* expressed in over 99% of the 6d HD (Q) population (Fig 3C). Some of these are previously identified stress-response genes (*SPG1*, and two orthologs, *GRE1 and SIP18* (Dang and Hincha 2011; Martinez et al. 2004; Miralles and Serrano 1995)) and four with partial (*TMA10, DDR2 (Fleischer et al. 2006; Kobayashi et al. 1996)*), or no characterization (*YKL065W-A, YER084W*). Individual deletion of these 7 genes

did not affect growth into quiescence, return to the cell cycle, telomere hypercluster formation and dismantling, or expression of the Hxt1 hexose transporter upon return to growth (Supplemental Fig. S3K). We hypothesize that these genes exert redundant functions or are important to resist specific stress conditions. These genes either have less RNAPII binding in abruptly starved cells, or they show a 5'-biased profile, as seen for *GRE1* (Fig. 3C). Thus, despite showing a genome-wide decrease in transcription, and similar nuclear morphology, the remaining transcription in quiescence can distinguish different methods of induction, as previously reported (Klosinska et al. 2011). Taken together, these results provide strong evidence for active transcription that is homogeneously retained in the highly dense population at 6 days for a set of 161 genes, with only a handful being widely and relatively strongly transcribed.

RNAPII re-distributes to a subset of promoter-bearing intergenes when cells enter quiescence

We noticed that entry into quiescence is accompanied by a redistribution of RNAPII away from gene bodies (Fig. 3A, C, gray boxes). When first induced at respiration or fermentation, class I genes show a canonical profile, with a TSS-proximal accumulation followed by increasing RNAPII enrichment towards the 3' end of coding sequences (Bataille et al. 2012; Mayer et al. 2010; Tietjen et al. 2010). But, as the culture approaches SP (day 2-HD) and increasingly as cells reach either quiescent state (Q or Q-like), Rpb3-FLAG is partially retained within the gene body while accumulating outside the ORF specifically in Q cells (Fig. 3A, C, gray boxes and below).

To ask whether RNAPII was enriched in Q in all intergenes alike, we sorted them based on the orientation of their surrounding annotations (convergent, divergent,

tandem) and examined their enrichment in RNAPII (Fig. 4A). As previously reported (Bataille et al. 2012; Mayer et al. 2010; Ocampo et al. 2019; Tietjen et al. 2010), during exponential growth (Log), RNAPII is highly enriched at convergent intergenes, and near the transcription start sites in tandem and divergent intergenes.

In sharp contrast, in Q samples, RNAPII is mostly enriched within the boundaries of those intergenes containing a promoter: tandem and divergent, the latter one being particularly striking, as these show virtually no enrichment in growing cells. Peak calling analysis, using the IP on untagged samples (FLAG on Rpb3 WT) as controls (methods), corroborates the significance of the observed enrichment (Supplemental Fig. S4A). Input and untagged IP (anti-FLAG on Rpb3 WT) chromatin coverage tracks show no enrichment or depletion at these locations, ruling out a potential artefact (Supplemental Fig. S4B). This was further confirmed by ChIP q-PCR (see below, Fig. 4B). Thus, RNAPII is depleted from convergent intergenes, while accumulating at 1773 promoter-bearing intergenes, upstream of 2478 genes in quiescent chromatin (Supplemental Fig. S4A, methods).

Promoter-bound RNAPII bears signs of canonical transcription

All epitopes of the RNAPII complex that we targeted using ChIP-qPCR follow the same trend of enrichment at promoters (Fig. 4B; Supplemental Fig. S4C), thereby indicating presence of the whole catalytic RNAPII. This was not the case for the FLAG-tagged Rpa135 subunit of RNAPI. As our ChIP-seq was performed against FLAG-tagged Rpb3 this allows to rule out a potential artefact owing from the *hyper-chippability* of the FLAG epitope at these loci (Teytelman et al. 2013). Furthermore, we detect the Rpb1 CTD phosphorylations (Ser2, 3E8; Ser5, 3E10), associated with elongation and initiation (Komarnitsky et al. 2000) in cycling cells, suggesting that

RNAPII may be active at these sites specifically in quiescence. Indeed, Ser5P is enriched at the *DCP2/MLS1* intergenic region where no Ser5P enrichment could be detected during log phase, though Rpb3 was clearly detected over the *DCP2* gene body. Ser5P was also found enriched in the promoter of the *ADY2* class I gene (Supplemental Fig. S4C) with levels three to six times higher than in the *DCP2/MLS1* intergene, possibly linked to the stronger activity of *ADY2* over *DCP2* or *MLS1*.

We next compared Rpb3-FLAG ChIP signal at the summits of peaks within promoter-containing intergenic regions (1442 upstream of 1940 genes,methods) with those of other factors previously mapped in quiescent chromatin (Cucinotta et al. 2021; Swygert et al. 2019; Guidi et al. 2015). As expected, the silencing factor Sir3 does not co-localize with Rpb3-FLAG (Fig. 4C), while ChIP-seq signal obtained with a native Rpb3 antibody does (Swygert et al., 2019). In contrast, Sth1 (RSC) showed low enrichment at these sites, while Rpb1-Ser2P, Brn1, Msn2, and especially TFIIB (Sua7) showed higher correlation with Rpb3-FLAG peaks. Notably, TFIIB binding suggests the presence of the pre-initiation complex (PIC) and closely follows RNAPII enrichment in quiescent chromatin. This pattern differs in cycling (Jeronimo and Robert 2014) (Fig. 4C, gray box) and refed quiescent cells (Cucinotta 2021) (Supplemental Fig. S4C), where TFIIB localizes near to but not at Rpb3-FLAG peaks.

The detection of Rpb1-Ser5P and TFIIB subunit Sua7 at intergenic Rpb3 peaks is indicative of active transcription. However, recently synthesized transcripts (4tU-seq, (Cucinotta et al. 2021)) are rarely found directly under the strongest summits (42/513). The absence of 4tU signal could stem from the lack of sensitivity to detect short or unstable transcripts. Yet, amongst all 1940 promoters showing Rpb3-FLAG peak summits in quiescence, half (945) are found upstream of genes with detectable

levels of newly synthesized transcripts (class I, p-value 2.23×10^{-03}, and class III genes, p-value 1.23×10^{-43}, Fig 4B, 4D).

In summary, RNAPII is found associated with PIC components and bearing marks indicative of activity at non-canonical sites, in the quiescent genome.

RNAPII accumulates at upstream activating sequences (UAS) during quiescence entry

Summits of strong peaks fall more often than expected within promoters bearing a fuzzy and or fragile nucleosome positioning (hypergeometric test, p-value= 2.1×10^{-36}, (Tirosh and Barkai 2008; Kubik et al. 2015)). Amongst the different classes of TF bound promoters defined by Rossi et al, 2021, strong peaks are enriched at those endowed with SAGA, Mediator or TUP cofactors (STM) (hypergeometric test, p-value=3.7×10^{-190}), and at Ribosomal Protein (RP) genes (hypergeometric test, p-value=6.2×10^{-20}). This was not the case at TFO promoters (TF organization lacking STM cofactors, and bound by insulators, p-value=0.19). RNAPII is thus enriched at inducible promoters in quiescent cells.

The binding of RNAPII skews towards the 3' end of all three classes (RP, STM and TFO) after cells undergo Diauxic Shift, reminiscent of the pattern reported for stationary phase cells by the Osley lab (Young et al. 2017). This is followed by a virtual depletion over the gene body that is accompanied by a progressive accumulation at the promoter of STM and RP genes but not at TFO genes from late post-diauxie to quiescence (Fig. 5A).

The strongest RNAPII enrichment lies at 250 bp from TSS in quiescence, where upstream activating sequences (UAS) are often found (Fig. 5B, Supplemental Fig. S5 A). Indeed, about 25% (125/513) of summits of strong peaks falling in promoters coincide with annotated UAS. Similarly, 111 binding motifs, encompassing a variety

of functions (methods), are found to be enriched in the vicinity (100 bp) of the strongest RNAPII summits.

Thus, RNAPII quiescent enrichment does not seem to result from a previously known program driven by a small set of regulators. Those motifs with a fold-enrichment over control greater than 3 are shown in Fig. 5C. Some sites are well-positioned near but not immediately under the RNAPII summit in quiescence (e.g., Rap1, Pdr3, Fig. S5C), and correspond to known regulators of genes highly expressed during growth (Rap1) or to factors involved in chromatin modifications associated with the shutdown of transcription upon quiescence entry (e.g. Snt2, recruiting factor for Rpd3, (Baker et al. 2013; McKnight et al. 2015)) or the remodeling of chromatin/maintenance of the NFR (e.g. Rsc3, Rsc30, (Badis et al. 2008)).

Some of the TFBS we found are puzzling, like those recognized by proteins of uncharacterized function (*YPR196W*, *YKL222C*, *YER184C*, *YNR063W* and *YER130C*), but also that of Gal4, as cells were presumably not exposed to galactose. In total, 220 genes with a significantly enriched RNAPII peak show virtually no sign of transcription during quiescence and quiescence entry. These include *GAL* genes (Supplemental Fig. S5A).

We next used *k*-means clustering to study the dynamics of RNAPII around all summits in promoter-bearing intergenes during quiescence entry (methods). The first group comprises 437 summits in Q-cells (Fig. 5D; supplemental Fig. S5B) where polymerase is enriched throughout the kinetics, starting from exponentially growing cells. The second group (601 summits) show weaker levels of RNAPII at the summit in log and early respiration phase (day 1). Note that one such Rpb3-FLAG summit is found at the intergene upstream of *ADY2,* together with the initiation Ser5-P

369 modification (Supplemental Fig. S4C). The third group (404 summits) is depleted of
370 signal in all growing phases (Log through day 1), and only starts increasing after day
371 2, as illustrated with *GAL7* (Fig. 5D; Supplemental Fig. S5C). Binding motifs highly
372 enriched under summits of the third group of peaks include binding factors known to
373 be active upon glucose de-repression (e.g. Adr1, Mig1,2,3 (Carlson 1999; Schüller
374 2003)), but also include a variety of factors involved in various responses, including,
375 again, Gal4 (Fig. 5C; Supplemental Fig. S5C). Abruptly starved cells either show a
376 lower enrichment of RNAPII at these regions (e.g. at *DDR2* promoter, Fig. 5C,
377 Supplemental Fig. S5B), or none (*e.g.* at *GAL7* promoter, Fig. 5D; Supplemental Fig.
378 S5A-B).
379 In summary, in contrast to genic binding of RNAPII in Q, that was already present as
380 cells were growing, a third of the intergenic enrichment found in starved cells is Q-
381 specific, increasing only after cells have been in culture for more than two days.

382 **Upstream RNAPII predicts strength of transcriptional re-start upon release**
383 We next asked whether promoter-bound RNAPII in quiescent chromatin would relate
384 to the swift re-start of transcription observed upon return to growth. We performed *k*-
385 means clustering to categorize 5778 genes based on the dynamics of newly
386 synthesized transcripts abundance 10 minutes after nutrient restoration (Cucinotta et
387 al. 2021) (Fig. 6A), thus identifying four groups: the first one comprises class I and
388 class III genes with transcripts in Q that show a decrease in relative labels of 4tU
389 incorporation upon release (Ø, 101 genes Fig. 6A; Supplemental Fig. S6A).
390 The other three groups (RI, 287 genes; RII, 2030 genes; RIII 3218 genes) show
391 decreasing levels of release probability (Supplemental Fig. S6B). The genes that
392 more robustly re-start (categories RI and RII) show the highest enrichment for genes
393 with an upstream RNAPII summit, amongst which are found most ribosomal protein

(RP) genes (Fig. 6A). Conversely, genes with a stronger upstream enrichment (with a RNAPII peak overlapping with their promoter) show higher 4tU counts upon release compared to those with a milder one or no detectable enrichment (Supplemental Fig. S6C).

Although 738 genes with upstream RNAPII summit show a milder upregulation 10 minutes after release with glucose, it is stronger than those without an RNAPII summit (cluster RIII, Fig. 6A; Supplemental Fig. S6D). These are mostly enriched in functions related to the metabolism of galactose and various alcohols, to which cells are not exposed in these feeding conditions (Supplemental Fig. S6E). In short, while not predicting the transcriptional program upon release, promoter-bound RNAPII predicts the strength of potential re-ignition of downstream genes.

To assess the heterogeneity of transcriptional activation across the cells and across release conditions, we performed single cell transcriptomes 30 min after diluting cells either in rich glucose (2%) or lactate (0.5 %) and ethanol (2%) medium. For both conditions, we found that genes with an RNAPII summit in their promoter in Q cells are highly enriched amongst the 10% most frequently expressed genes (Fig. 6B; Supplemental Fig. S6F) corresponding to genes detected in 32-98% of cells in glucose and 22-97% of cells in lactate-ethanol (Supplemental Fig. S6G). This suggests that promoter-bound RNAPII marks genes that can be pervasively transcribed in the population when quiescent cells are refed.

Pervasively transcribed genes with an RNAPII peak in their promoter highly overlap (Fig 6B) between the two conditions, suggesting that, regardless of the available sugar, cells engage in a common program in the early stages of quiescence release. These common genes are enriched in protein synthesis functions (Supplemental Fig S6H), including Ribi and RP genes. However, 24% of the promoter-bound RNAPII

showing pervasive transcription upon release in lactate ethanol are not pervasively expressed in glucose. These are enriched for functions related to respiration (Supplemental Fig. S6H) and include the gluconeogenesis gene *PYC1*. Therefore, RNAPII peaks in promoter regions marks genes that can be mobilized differently to adapt to distinct environments.

DISCUSSION

We investigated the relationship between telomere clustering and transcriptional dynamics during quiescence entry and return to growth. We show that transcriptional shut-down is partial and precedes telomere hyperclustering during quiescence entry. Similarly, transcriptional upregulation occurs before the dismantling of telomere hyperclustering upon return to growth. Yet we show that these two dynamics are independent. This is reminiscent of rod cell nuclei of nocturnal mammals, that show a similar internalization of heterochromatin that is not accompanied by notable effects on genome expression (Solovei et al. 2009).

We also report a distinct, transcriptionally idle quiescent chromatin landscape, holding at promoters the potential for prompt restart in the form of RNAPII accumulation.

Quiescent chromatin is not transcriptionally inert

We report a two-fold increase in RNAPII binding at the rDNA, together with a three-fold decrease in the rest of the genome. Our calibrated ChIP-seq study, integrated with metabolically labeled transcriptomic data (Cucinotta et al. 2021), provides strong evidence for active transcription of 3% of protein-coding genes (class I), thus showing that quiescent cells are not transcriptionally inert. The sensitivity of 4tU-labeled transcript detection and RNAPII ChIP might cause an underestimation, and the actual figure could be up to 35,7% if considering only 4tU-signal.

RNAPII re-distributes to promoter-bearing intergenes over several days

Although transcriptional shut down is observed after 2 days of culture, RNAPII binding continues to evolve at least until day 6, with different gene body association of RNAPII and its progressive accumulation at UAS of RP genes and inducible STM genes. Consistently, we observe a stronger intergenic RNAPII accumulation in

quiescent cells resulting from medium exhaustion than in quiescent cells resulting from post-diauxic shift starvation.

Previous assessments of polymerase binding to quiescent chromatin were conflicting, with recent studies reporting a lack of enrichment at intergenes. Unlike Radonjic et al., who detected intergenic enrichment in unsorted stationary phase populations, Young et al. found a bias towards the 3' of CDS. This distribution correlates best with our early post-diauxic shift samples, suggesting a difference in the kinetics of quiescence entry, likely due to differences in growth conditions such as aeration and medium pH (Greenlaw et al. 2024; Opalek et al. 2023). Data from the Tsukiyama laboratory, however, agree with our findings (Swygert et al. 2019 and Supplemental Fig. S4C). Some of the reported discrepancies (Cucinotta et al. 2021) could be attributed to differential efficiency in immunoprecipitation, as tagged epitopes can lead to better enrichments, as previously reported (Hu et al. 2015; Jeronimo and Robert 2014). Finally, we observed the enrichment of the condensin subunit Brn1 (Swygert et al. 2019) at RNAPII Q peaks, in good agreement with published data showing the accumulation of condensin at RNAPII bound sites in other conditions (D'Ambrosio et al. 2008).

Bookmarking genes in quiescent yeast

Evidence for RNAPII pausing in budding yeast is limited, leading to the general belief that it does not occur. Although the Negative Elongation Factor (NELF) — absent in budding yeast — is linked to stable transcriptional pausing, it is not essential as shown in *S. pombe* (Booth et al. 2018; Core and Adelman 2019). To our knowledge, few reports of promoter-proximal seemingly inactive RNAPII, with the potential to reactivate, exist in budding yeast. RNAPII remains at the *INO1* promoter for hours post-repression, enhancing reactivation upon reinduction and indicating epigenetic

memory (DG Brickner 2007, Brickner & Walter 2004, Light et al., 2010). Such bookmarking may explain RNAPII presence upstream of genes transcribed during quiescence entry.

However, 220/1910 genes with an upstream RNAPII peak are not transcribed during quiescence entry, including *GAL* genes. This is reminiscent of RNAPII found together with PIC components, at promoters made accessible by the absence of Hda1 and Rpd3 deacetylases, in a state favorable for activation under Snf1 control (Tachibana et al. 2007, 2005).

Such an activation-prone state is consistent with our observation of RNAPII mostly upstream of genes seemingly ready to be highly transcribed within minutes of refeeding in at least two different conditions.

Using ATP analog-sensitive mutants (kin28-as) (Bataille et al. 2012; Jeronimo and Robert 2014; Tietjen et al. 2010) or anchor-away depletion (Wong et al. 2014) to inhibit Kin28 results in RNAPII accumulation at core promoters. RNAPII accumulation in quiescence, however, tends to occur 250 bp upstream of the TSS, further upstream than that typically observed in cycling cells (Bataille et al. 2012; Jeronimo and Robert 2014; Kubik et al. 2019; Mayer et al. 2010; Pelechano et al. 2014; Steinmetz et al. 2006), and rather coinciding with reported locations for Mediator at UAS (Andrau et al. 2006; Ansari et al. 2009; Fan et al. 2006; Jeronimo and Robert 2014). Possibly related to our finding, Mediator subunits also accumulate at UAS of RP genes upon heat-shock (Sarkar et al. 2022).

Although our crosslinked chromatin mapping cannot exclude some enzyme proximity rather than DNA binding, recent studies using improved detection methods for engaged polymerase and small transcripts have mapped RNAPII at similar distances from the canonical PIC assembly (Xi et al. 2024), suggesting RNAPII recruitment

may occur at UAS in cycling cells. Consistently, RNAPII intergenic signal can be detected at two thirds of the quiescent peaks in growing cells, although not forming well-defined peaks. Furthermore, we detect some Ser5-P CTD phosphorylation at some of these intergenic peaks in Q cells, suggesting that at least some RNAPII might be active at these loci.

These observations are in agreement with *in vitro* studies showing transient RNA pol II interaction at activator-bound UAS before loading into the core promoter (Baek et al. 2021). Although RNAPII binding is not detected at UAS by ChIP in exponentially growing cells it is clearly detected by ChEC-Seq2 at active STM genes (VanBelzen et al. 2024). The weak general levels of transcription in quiescent cells may uncover binding sites otherwise difficult to detect by ChIP in growing cells.

RSC was proposed to enable newly recruited RNAPII to progress into gene bodies upon release (Cucinotta et al. 2021). Furthermore, re-entry into cell cycle is delayed (Cucinotta et al. 2021) in the absence of the general transcription elongation factor TFIIS (Dst1) (Kettenberger et al. 2003; Kireeva and Kashlev 2009; Wery et al. 2004). Our results indicate that these factors favor transcription from RNAPII accumulated upstream of genes during quiescence.

We hypothesize that the odd RNAPII ChIP profile at these genes stems from altered dynamics of the transcription cycle, wherein RNAPII would bind UAS, only rarely engaging in transcription along the gene body. This idea is well supported with the recently published kinetic model of RNAPII transcription (VanBelzen et al. 2024). Such idle, minimal, activity would occur stochastically in the population, contributing to maintain a responsive quiescent chromatin, that can be mobilized differently to adapt to distinct environments.

METHODS

Strains and growth conditions

All *S. cerevisiae* strains used in this study, haploid (mating type a) and isogenic to the W303 background, are listed in Supplemental Table S1. Gene targeting for gene deletion and gene tagging was performed as described in (Longtine et al. 1998). Cells were inoculated in YPD (yeast-peptone-dextrose 2%) and grown overnight before diluting to 0.1 OD_{600}/mL to start the kinetics of entry into quiescence. Cells were grown at 30°C (except *rpb1-1* strains that were grown at 25°C), shaking at 250 rpm, at 1/10 volume in glass flasks with aeration caps. Diauxic shift samples were harvested two hours after glucose was no longer detectable in the medium, when transcriptional changes are detectable (Brauer et al. 2008). To induce quiescence by nutrient exhaustion (Q 6d-HD), cells were grown to reach stationary phase (50-60 OD_{600}/mL) at 30 °C, then gradient-enriched in HD cells (see below). To induce quiescence by abrupt starvation (Q-like), cells were grown in YPD as described above for 24h, then gradient-sorted (see below), and the recovered HD fraction was resuspended in sterile H2O, then incubated at 30 °C, shaking, for another 24 hours. The *S. pombe* strain used as spike-in for ChIP-seq was grown in YES medium (yeast extract supplemented) to mid-log phase, in parallel to mid-log phase *S. cerevisiae* samples (0.4-0.7 OD_{600}/mL). For release from quiescence experiments, HD cells were enriched from a 6 days stationary phase culture, washed in H_2O and incubated overnight at 30ºC, under shaking. Then, they were re-suspended at 1 OD/mL in fresh YPD at 1:10 volume:air ratio for the indicated times. For single cell experiments, cells were released in either YPD (2% glucose) or YPLE (0.5%Lactate, 2% Ethanol). To recover mainly the highly dense population as cells progress into stationary phase in the nutrient exhaustion kinetics, all samples after diauxic shift

(24h, 48h, Q-like, Q6d) were gradient sorted, based on the principle described in (Allen et al. 2006). A detailed procedure is described in Supplemental Materials and Methods

Transcription inhibition experiments

Transcription inhibition experiments were carried out on stationary phase culture (7 d) or HD-enriched (quiescent) culture, as indicated in the corresponding figure. *rpb1-1* cells were grown to stationary phase at 25°C. Cells were pretreated for 2 hours with the inhibitor (thiolutin SIGMA, final concentration at 10µg/mL, or phenanthroline 100µg/ml final, stock solutions in DMSO) or preincubated for 1 hour at 37°C for the *rpb1-1* strain. For each condition, 6×10^7 cells (1 OD/mL) were released in fresh YPD only, or in the presence of the corresponding inhibitor or temperature. Then, cultures were sampled after 30, 60 and 120 minutes of incubation, shaking, at 25°C, 30°C or 37°C as indicated in the figure legend. For wash-out, all samples, including controls, were washed 3 times in PBS1× and re-suspended in fresh YPD only, then imaged after 30, 90, 120 and 240 minutes.

Imaging and Rap1-GFP foci quantification

Samples were harvested at the indicated timepoints, rinsed in H_2O and placed on a 4% agarose patch before imaging. Image acquisition was performed as described in Guidi et al. 2015, with modifications described in Supplemental Materials and Methods. Image analysis relied on our custom-made software (https://github.com/mgPICT/NuFoQ), which was adapted from Guidi et al. 2015 to enable three-dimensional (3D) segmentation and quantification of nuclear foci. Further details can be found in the Supplemental Materials and Methods section.

Sample harvesting for chromatin immunoprecipitation

For every timepoint in the kinetics of quiescence entry, 100 OD_{600} of cells were harvested for chromatin immunoprecipitation. An aliquot from the same sample was washed in H_2O and placed on a 4% agarose patch before imaging. For each of the two biological replicates, WT Rpb3 (yAT1684) and FLAG-tagged (yAT3239, yAT3555) strains were grown with the same batch of YPD and processed together for chromatin immunoprecipitation and imaging. Chromatin immunoprecipitation experiments, described in detail in Supplemental Materials and Methods, were performed as described in (Guidi et al. 2015; Ruault et al. 2021). qPCR primers are listed in Supplemental Table S2.

ChIP-seq data processing

Rpb3-FLAG ChIP-seq libraries were sequenced (single-end 50 (HiSeq-Rapid Run)) at the Institut Curie NGS platform. WT samples (yAT1684 and yAT3239) were sequenced together. WT IP samples for Log and Q (6dHD) were re-sequenced together with *sir3Δ* samples in a different run. Thus, they were treated separately for analysis. For mapping, reads were competitively aligned to a hybrid *S. pombe* (ASM294v2.28) and *S. cerevisiae* genome (SGD Project 2015), with Bowtie 2 (bowtie2-align-s -p 8, (Langmead and Salzberg 2012)). To visualize sub-telomeric genes, filtering was performed to allow up to three mismatches (grep -E "(^@|XM:i:[0-3])").

To calibrate the ChIP signal, an occupancy ratio (OR) was calculated based on the number of uniquely mapped reads to either genome (experimental: *S.cerevisiae*, spike-in: *S. pombe*), present in IP and INPUT samples of the Rpb3-FLAG tagged (yAT3239) and Rpb3 untagged (yAT1684) strains, as described in (Hu et al. 2015). OR was used as a scaling factor to generate coverage tracks from IP samples (shown in all genome browser snapshots, and average profile plots, except when

compared to other mappings, in Fig. 4D and Supplemental Fig. S4C, see below), using deepTools (3.5.0) (Ramírez et al. 2016) BamCoverage with RPKM normalization. The coverage for all IP and INPUT samples is depicted in Supplemental Fig. S4B.

scRNA-seq experiments

Single-cell encapsulation and libraries preparation were performed using the SingleCell3'-10× technology. For cell harvesting and counting, we adapted the 10× demonstrated protocol for methanol fixation (available upon request from 10× Genomics, and described in more detail in Supplemental Materials and Methods). For cell encapsulation, steps 1.2d-e of the 10× Genomics single cell protocol version v3.1 were modified as follows: a gel beads and zymolyase suspension was prepared. A 100× stock of zymolyase (100 mg/mL, MP Biomedicals, 8320932) solution was added to the gel beads suspension to reach 1.7× final concentration before loading on the chip. Note that previous studies in growing cells (Vermeersch et al. 2022; Jariani et al. 2020) have used 1× concentration, but that, for quiescent cells, this was not sufficient. Then, 50 µL of gel beads and zymolyase suspension were dispensed as indicated into row labeled 2 of the chip, before proceeding with library preparation according to protocol. Samples were sequenced in a NovaSeq (PE28-10-10-90).

RNA-seq experiments

25 OD600nm equivalent of cells were harvested, pelleted, flash-frozen and stored at -70º before processing with Ribopure Yeast RNA (invitrogen AM1926). Directional mRNA libraries (poly(A) enrichment) were processed and paired-end sequenced by Novogene Europe.

Data processing

625 ChIP-seq, scRNA-seq and RNA-seq data processing details are described in
626 Supplemental Materials and Methods. Promoter-bearing intergenes (Fig 4)
627 overlapped by RNAPII peaks are listed in Supplemental Table S3. Rpb3-FLAG
628 peaks' summits falling in promoter-bearing intergenes (Fig 4) are listed in
629 Supplemental Table S4. TFBS enriched in the vicinity (100 bp) of the strongest
630 RNAPII summits (Fig 5) are listed in Supplemental Table S5. R packages used for
631 analyses are listed in Supplemental Table S6.
632

633 DATA ACCESS

634 The Rpb3-FLAG ChIP-seq, scRNA-seq and RNA-seq data generated in this study
635 have been submitted to EMBL-EBI ArrayExpress
636 https://www.ebi.ac.uk/biostudies/arrayexpress under accession numbers E-MTAB-
637 14337, E-MTAB-14980, E-MTAB-14983.
638

639 COMPETING INTEREST STATEMENT

640 The authors declare that they have no known competing interests.

641 ACKNOWLEDGEMENTS

642 The authors thank the members of the Taddei laboratory and of UMR3664 for helpful
643 discussions. The A.T. team was financially supported by funding from the Labex
644 DEEP (ANR-11-LABEX-0044 DEEP and ANR-10IDEX-0001-02 PSL), from the
645 Agence Nationale de la Recherche DNA-Life (ANR-15-CE12-0007) and DeSynLE
646 (ANR-22-CE12-0013-01). M.B.P. was supported in part by a fellowship from Institut
647 Curie (IC3i 2019) and by the Labex DEEP (ANR-11-LABEX-0044 DEEP).

Most bioinformatic analyses were performed on the Core Cluster of the Institut Français de Bioinformatique (IFB) (ANR-11-INBS-0013), using an estimated 4762.68 hours per CPU. The authors also thank the PICT-IBiSA@Pasteur Imaging Facility of the Institut Curie, a member of the France Bioimaging National Infrastructure (ANR-10-INBS-04).

AUTHOR CONTRIBUTIONS

I.L., M.B.P. and M.R. generated strains. M.B.P and M.R performed ChIP-seq experiments. M.B.P, M.R., and I.L. carried out imaging and ChIP-qPCR experiments. M.G. generated the software to quantify microscopy images. M.B.P. and U.S. processed ChIP-seq data. M.B.P and G.L performed scRNA-seq experiments. G.L. carried out scRNA-seq analyses. G.L. performed RNA-seq experiments. M.B.P. carried out all other bioinformatic analyses. A.T., M.R., A.M., G.L., and M.B.P contributed to the design of the experiments. A.T. and A.M. obtained funding. A.T., and M.B.P. contributed to the interpretation of the data, the drafting of the figures, and the writing/revision of the manuscript.

REFERENCES

Abruzzi KC, Belostotsky DA, Chekanova JA, Dower K, Rosbash M. 2006. 3′-end formation signals modulate the association of genes with the nuclear periphery as well as mRNP dot formation. *EMBO J* **25**: 4253–4262.

Allen C, Büttner S, Aragon AD, Thomas JA, Meirelles O, Jaetao JE, Benn D, Ruby SW, Veenhuis M, Madeo F, et al. 2006. Isolation of quiescent and nonquiescent cells from yeast stationary-phase cultures. *J Cell Biol* **174**: 89–100.

Andrau J-C, van de Pasch L, Lijnzaad P, Bijma T, Koerkamp MG, van de Peppel J, Werner M, Holstege FCP. 2006. Genome-wide location of the coactivator mediator: Binding without activation and transient Cdk8 interaction on DNA. *Mol Cell* **22**: 179–192.

Ansari SA, He Q, Morse RH. 2009. Mediator complex association with constitutively transcribed genes in yeast. *Proc Natl Acad Sci U S A* **106**: 16734–16739.

Aragon AD, Quiñones GA, Thomas EV, Roy S, Werner-Washburne M. 2006. Release of extraction-resistant mRNA in stationary phase Saccharomyces cerevisiae produces a massive increase in transcript abundance in response to stress. *Genome Biol* **7**: R9.

Aragon AD, Rodriguez AL, Meirelles O, Roy S, Davidson GS, Tapia PH, Allen C, Joe R, Benn D, Werner-Washburne M. 2008. Characterization of differentiated quiescent and nonquiescent cells in yeast stationary-phase cultures. *Mol Biol Cell* **19**: 1271–1280.

Badis G, Chan ET, Bakel H van, Pena-Castillo L, Tillo D, Tsui K, Carlson CD, Gossett AJ, Hasinoff MJ, Warren CL, et al. 2008. A Library of Yeast Transcription Factor Motifs Reveals a Widespread Function for Rsc3 in Targeting Nucleosome Exclusion at Promoters. *Mol Cell* **32**: 878–887.

684 Baek I, Friedman LJ, Gelles J, Buratowski S. 2021. Single-molecule studies reveal branched
685 pathways for activator-dependent assembly of RNA polymerase II pre-initiation
686 complexes. *Mol Cell* **81**: 3576-3588.e6.

687 Bailey TL, Grant CE. 2021. SEA: Simple Enrichment Analysis of motifs.
688 2021.08.23.457422. https://www.biorxiv.org/content/10.1101/2021.08.23.457422v1
689 (Accessed July 29, 2024).

690 Baker LA, Ueberheide BM, Dewell S, Chait BT, Zheng D, Allis CD. 2013. The yeast Snt2
691 protein coordinates the transcriptional response to hydrogen peroxide-mediated
692 oxidative stress. *Mol Cell Biol* **33**: 3735–3748.

693 Bataille AR, Jeronimo C, Jacques P-É, Laramée L, Fortin M-È, Forest A, Bergeron M, Hanes
694 SD, Robert F. 2012. A Universal RNA Polymerase II CTD Cycle Is Orchestrated by
695 Complex Interplays between Kinase, Phosphatase, and Isomerase Enzymes along
696 Genes. *Mol Cell* **45**: 158–170.

697 Booth GT, Parua PK, Sansó M, Fisher RP, Lis JT. 2018. Cdk9 regulates a promoter-proximal
698 checkpoint to modulate RNA polymerase II elongation rate in fission yeast. *Nat*
699 *Commun* **9**: 543.

700 Bourbousse C, Barneche F, Laloi C. 2020. Plant Chromatin Catches the Sun. *Front Plant Sci*
701 **10**. https://www.frontiersin.org/articles/10.3389/fpls.2019.01728 (Accessed October
702 11, 2023).

703 Brauer MJ, Huttenhower C, Airoldi EM, Rosenstein R, Matese JC, Gresham D, Boer VM,
704 Troyanskaya OG, Botstein D. 2008. Coordination of Growth Rate, Cell Cycle, Stress
705 Response, and Metabolic Activity in Yeast ed. T. Fox. *Mol Biol Cell* **19**: 352–367.

706 Brickner JH, Walter P. 2004. Gene recruitment of the activated INO1 locus to the nuclear
707 membrane. *PLoS Biol* **2**: e342.

708 Candelli T, Challal D, Briand J-B, Boulay J, Porrua O, Colin J, Libri D. 2018. High-
709 resolution transcription maps reveal the widespread impact of roadblock termination
710 in yeast. *EMBO J* **37**: e97490.

711 Carlson M. 1999. Glucose repression in yeast. *Curr Opin Microbiol* **2**: 202–207.

712 Casolari JM, Brown CR, Komili S, West J, Hieronymus H, Silver PA. 2004. Genome-wide
713 localization of the nuclear transport machinery couples transcriptional status and
714 nuclear organization. *Cell* **117**: 427–439.

715 Castro-Mondragon JA, Riudavets-Puig R, Rauluseviciute I, Berhanu Lemma R, Turchi L,
716 Blanc-Mathieu R, Lucas J, Boddie P, Khan A, Manosalva Pérez N, et al. 2022.
717 JASPAR 2022: the 9th release of the open-access database of transcription factor
718 binding profiles. *Nucleic Acids Res* **50**: D165–D173.

719 Cioci F, Vu L, Eliason K, Oakes M, Siddiqi IN, Nomura M. 2003. Silencing in Yeast rDNA
720 Chromatin: Reciprocal Relationship in Gene Expression between RNA Polymerase I
721 and II. *Mol Cell* 11.

722 Core L, Adelman K. 2019. Promoter-proximal pausing of RNA polymerase II: a nexus of
723 gene regulation. *Genes Dev* **33**: 960–982.

724 Cucinotta CE, Dell RH, Braceros KC, Tsukiyama T. 2021. RSC primes the quiescent genome
725 for hypertranscription upon cell-cycle re-entry eds. T. Formosa, J.K. Tyler, and T.
726 Formosa. *eLife* **10**: e67033.

727 D'Ambrosio C, Schmidt CK, Katou Y, Kelly G, Itoh T, Shirahige K, Uhlmann F. 2008.
728 Identification of cis-acting sites for condensin loading onto budding yeast
729 chromosomes. *Genes Dev* **22**: 2215–2227.

730 Dang NX, Hincha DK. 2011. Identification of two hydrophilins that contribute to the
731 desiccation and freezing tolerance of yeast (Saccharomyces cerevisiae) cells.
732 *Cryobiology* **62**: 188–193.

733 Davidson GS, Joe RM, Roy S, Meirelles O, Allen CP, Wilson MR, Tapia PH, Manzanilla EE,
734 Dodson AE, Chakraborty S, et al. 2011. The proteomics of quiescent and
735 nonquiescent cell differentiation in yeast stationary-phase cultures. *Mol Biol Cell* **22**:
736 988–998.

737 DeRisi JL. 1997. Exploring the Metabolic and Genetic Control of Gene Expression on a
738 Genomic Scale. *Science* **278**: 680–686.

739 Eshleman N, Luo X, Capaldi A, Buchan JR. 2020. Alterations of signaling pathways in
740 response to chemical perturbations used to measure mRNA decay rates in yeast. *RNA*
741 *N Y N* **26**: 10–18.

742 Fan X, Chou DM, Struhl K. 2006. Activator-specific recruitment of Mediator in vivo. *Nat*
743 *Struct Mol Biol* **13**: 117–120.

744 Feodorova Y, Falk M, Mirny LA, Solovei I. 2020. Viewing Nuclear Architecture through the
745 Eyes of Nocturnal Mammals. *Trends Cell Biol* **30**: 276–289.

746 Fleischer TC, Weaver CM, McAfee KJ, Jennings JL, Link AJ. 2006. Systematic identification
747 and functional screens of uncharacterized proteins associated with eukaryotic
748 ribosomal complexes. *Genes Dev* **20**: 1294–1307.

749 Fuge EK, Braun EL, Werner-Washburne M. 1994. Protein synthesis in long-term stationary-
750 phase cultures of Saccharomyces cerevisiae. *J Bacteriol* **176**: 5802–5813.

751 Galitski T, Saldanha AJ, Styles CA, Lander ES, Fink GR. 1999. Ploidy Regulation of Gene
752 Expression. *Science* **285**: 251–254.

753 Gasch AP, Werner-Washburne M. 2002. The genomics of yeast responses to environmental
754 stress and starvation. *Funct Integr Genomics* **2**: 181–192.

755 Gray JV, Petsko GA, Johnston GC, Ringe D, Singer RA, Werner-Washburne M. 2004.
756 “Sleeping Beauty”: Quiescence in Saccharomyces cerevisiae. *Microbiol Mol Biol Rev*
757 **68**: 187–206.

758 Greenlaw A, Dell R, Tsukiyama T. 2024. Initial acidic media promotes quiescence entry in
759 Saccharomyces cerevisiae. *MicroPublication Biol* **2024**.

760 Guidi M, Ruault M, Marbouty M, Loïodice I, Cournac A, Billaudeau C, Hocher A,
761 Mozziconacci J, Koszul R, Taddei A. 2015. Spatial reorganization of telomeres in
762 long-lived quiescent cells. *Genome Biol* **16**: 206.

763 Hu B, Petela N, Kurze A, Chan K-L, Chapard C, Nasmyth K. 2015. Biological
764 chromodynamics: a general method for measuring protein occupancy across the
765 genome by calibrating ChIP-seq. *Nucleic Acids Res* **43**: e132.

766 Jariani A, Vermeersch L, Cerulus B, Perez-Samper G, Voordeckers K, Van Brussel T,
767 Thienpont B, Lambrechts D, Verstrepen KJ. 2020. A new protocol for single-cell
768 RNA-seq reveals stochastic gene expression during lag phase in budding yeast eds. A.
769 Rokas and N. Barkai. *eLife* **9**: e55320.

770 Jeronimo C, Robert F. 2014. Kin28 regulates the transient association of Mediator with core
771 promoters. *Nat Struct Mol Biol* **21**: 449–455.

772 Jona G, Choder M, Gileadi O. 2000. Glucose starvation induces a drastic reduction in the
773 rates of both transcription and degradation of mRNA in yeast. *Biochim Biophys Acta*
774 *BBA - Gene Struct Expr* **1491**: 37–48.

775 Kettenberger H, Armache K-J, Cramer P. 2003. Architecture of the RNA polymerase II-TFIIS
776 complex and implications for mRNA cleavage. *Cell* **114**: 347–357.

777 Kireeva ML, Kashlev M. 2009. Mechanism of sequence-specific pausing of bacterial RNA
778 polymerase. *Proc Natl Acad Sci U S A* **106**: 8900–8905.

779 Klosinska MM, Crutchfield CA, Bradley PH, Rabinowitz JD, Broach JR. 2011. Yeast cells
780 can access distinct quiescent states. *Genes Dev* **25**: 336–349.

781 Kobayashi N, McClanahan TK, Simon JR, Treger JM, McEntee K. 1996. Structure and
782 functional analysis of the multistress response gene DDR2 from Saccharomyces
783 cerevisiae. *Biochem Biophys Res Commun* **229**: 540–547.

784 Komarnitsky P, Cho E-J, Buratowski S. 2000. Different phosphorylated forms of RNA
785 polymerase II and associated mRNA processing factors during transcription. *Genes*
786 *Dev* **14**: 2452–2460.

787 Kubik S, Bruzzone MJ, Challal D, Dreos R, Mattarocci S, Bucher P, Libri D, Shore D. 2019.
788 Opposing chromatin remodelers control transcription initiation frequency and start
789 site selection. *Nat Struct Mol Biol* **26**: 744–754.

790 Kubik S, Bruzzone MJ, Jacquet P, Falcone J-L, Rougemont J, Shore D. 2015. Nucleosome
791 Stability Distinguishes Two Different Promoter Types at All Protein-Coding Genes in
792 Yeast. *Mol Cell* **60**: 422–434.

793 Langmead B, Salzberg SL. 2012. Fast gapped-read alignment with Bowtie 2. *Nat Methods* **9**:
794 357–359.

795 Laporte D, Courtout F, Salin B, Ceschin J, Sagot I. 2013. An array of nuclear microtubules
796 reorganizes the budding yeast nucleus during quiescence. *J Cell Biol* **203**: 585–594.

797 Lauinger L, Li J, Shostak A, Cemel IA, Ha N, Zhang Y, Merkl PE, Obermeyer S, Stankovic-
798 Valentin N, Schafmeier T, et al. 2017. Thiolutin is a zinc chelator that inhibits the
799 Rpn11 and other JAMM metalloproteases. *Nat Chem Biol* **13**: 709–714.

800 Longtine MS, Mckenzie III A, Demarini DJ, Shah NG, Wach A, Brachat A, Philippsen P,
801 Pringle JR. 1998. Additional modules for versatile and economical PCR-based gene
802 deletion and modification in Saccharomyces cerevisiae. *Yeast* **14**: 953–961.

803 Martinez MJ, Roy S, Archuletta AB, Wentzell PD, Anna-Arriola SS, Rodriguez AL, Aragon
804 AD, Quiñones GA, Allen C, Werner-Washburne M. 2004. Genomic analysis of
805 stationary-phase and exit in Saccharomyces cerevisiae: gene expression and
806 identification of novel essential genes. *Mol Biol Cell* **15**: 5295–5305.

807 Mayer A, Lidschreiber M, Siebert M, Leike K, Söding J, Cramer P. 2010. Uniform transitions
808 of the general RNA polymerase II transcription complex. *Nat Struct Mol Biol* **17**:
809 1272–1278.

McKnight JN, Boerma JW, Breeden LL, Tsukiyama T. 2015. Global Promoter Targeting of a Conserved Lysine Deacetylase for Transcriptional Shutoff during Quiescence Entry. *Mol Cell* **59**: 732–743.

Miles S, Bradley GT, Breeden LL. 2021. The budding yeast transition to quiescence. *Yeast* **38**: 30–38.

Miles S, Li L, Davison J, Breeden LL. 2013. Xbp1 directs global repression of budding yeast transcription during the transition to quiescence and is important for the longevity and reversibility of the quiescent state. *PLoS Genet* **9**: e1003854.

Miralles VJ, Serrano R. 1995. A genomic locus in Saccharomyces cerevisiae with four genes up-regulated by osmotic stress. *Mol Microbiol* **17**: 653–662.

Ocampo J, Chereji RV, Eriksson PR, Clark DJ. 2019. Contrasting roles of the RSC and ISW1/CHD1 chromatin remodelers in RNA polymerase II elongation and termination. *Genome Res* **29**: 407–417.

Opalek M, Tutaj H, Pirog A, Smug BJ, Rutkowska J, Wloch-Salamon D. 2023. A Systematic Review on Quiescent State Research Approaches in S. cerevisiae. *Cells* **12**: 1608.

Pelechano V, Wei W, Jakob P, Steinmetz LM. 2014. Genome-wide identification of transcript start and end sites by transcript isoform sequencing. *Nat Protoc* **9**: 1740–1759.

Qiu C, Arora P, Malik I, Laperuta AJ, Pavlovic EM, Ugochukwu S, Naik M, Kaplan CD. 2024. Thiolutin has complex effects in vivo but is a direct inhibitor of RNA polymerase II in vitro. *Nucleic Acids Res* **52**: 2546–2564.

Radonjic M, Andrau J-C, Lijnzaad P, Kemmeren P, Kockelkorn TTJP, van Leenen D, van Berkum NL, Holstege FCP. 2005. Genome-Wide Analyses Reveal RNA Polymerase

II Located Upstream of Genes Poised for Rapid Response upon S. cerevisiae Stationary Phase Exit. *Mol Cell* **18**: 171–183.

Ramírez F, Ryan DP, Grüning B, Bhardwaj V, Kilpert F, Richter AS, Heyne S, Dündar F, Manke T. 2016. deepTools2: a next generation web server for deep-sequencing data analysis. *Nucleic Acids Res* **44**: W160-165.

Rossi MJ, Kuntala PK, Lai WKM, Yamada N, Badjatia N, Mittal C, Kuzu G, Bocklund K, Farrell NP, Blanda TR, et al. 2021. A high-resolution protein architecture of the budding yeast genome. *Nature* **592**: 309–314.

Ruault M, Scolari VF, Lazar-Stefanita L, Hocher A, Loïodice I, Koszul R, Taddei A. 2021. Sir3 mediates long-range chromosome interactions in budding yeast. *Genome Res* **31**: 411–425.

Sarkar D, Zhu ZI, Knoll ER, Paul E, Landsman D, Morse RH. 2022. Mediator dynamics during heat shock in budding yeast. *Genome Res* **32**: 111–123.

Schäfer G, McEvoy CRE, Patterton H-G. 2008. The Saccharomyces cerevisiae linker histone Hho1p is essential for chromatin compaction in stationary phase and is displaced by transcription. *Proc Natl Acad Sci U S A* **105**: 14838–14843.

Schofield JA, Hahn S. 2023. Broad compatibility between yeast UAS elements and core promoters and identification of promoter elements that determine cofactor specificity. *Cell Rep* **42**: 112387.

Schüller H-J. 2003. Transcriptional control of nonfermentative metabolism in the yeast Saccharomyces cerevisiae. *Curr Genet* **43**: 139–160.

SGD Project. 2015. S288C_reference_genome_R64-2-1_20150113.tgz. http://sgd-archive.yeastgenome.org/sequence/S288C_reference/genome_releases/S288C_reference_genome_R64-2-1_20150113.tgz (Accessed June 30, 2019).

Solovei I, Kreysing M, Lanctôt C, Kösem S, Peichl L, Cremer T, Guck J, Joffe B. 2009. Nuclear Architecture of Rod Photoreceptor Cells Adapts to Vision in Mammalian Evolution. *Cell* **137**: 356–368.

Steinmetz EJ, Warren CL, Kuehner JN, Panbehi B, Ansari AZ, Brow DA. 2006. Genome-Wide Distribution of Yeast RNA Polymerase II and Its Control by Sen1 Helicase. *Mol Cell* **24**: 735–746.

Swygert SG, Kim S, Wu X, Fu T, Hsieh T-H, Rando OJ, Eisenman RN, Shendure J, McKnight JN, Tsukiyama T. 2019. Condensin-Dependent Chromatin Compaction Represses Transcription Globally during Quiescence. *Mol Cell* **73**: 533-546.e4.

Swygert SG, Lin D, Portillo-Ledesma S, Lin P-Y, Hunt DR, Kao C-F, Schlick T, Noble WS, Tsukiyama T. 2021. Local chromatin fiber folding represses transcription and loop extrusion in quiescent cells eds. G.J. Narlikar, K. Struhl, and V. Ramani. *eLife* **10**: e72062.

Tachibana C, Biddick R, Law GL, Young ET. 2007. A Poised Initiation Complex Is Activated by SNF1. *J Biol Chem* **282**: 37308–37315.

Tachibana C, Yoo JY, Tagne J-B, Kacherovsky N, Lee TI, Young ET. 2005. Combined global localization analysis and transcriptome data identify genes that are directly coregulated by Adr1 and Cat8. *Mol Cell Biol* **25**: 2138–2146.

874 Taddei A, Van Houwe G, Hediger F, Kalck V, Cubizolles F, Schober H, Gasser SM. 2006.
875 Nuclear pore association confers optimal expression levels for an inducible yeast
876 gene. *Nature* **441**: 774–778.

877 Teytelman L, Thurtle DM, Rine J, van Oudenaarden A. 2013. Highly expressed loci are
878 vulnerable to misleading ChIP localization of multiple unrelated proteins. *Proc Natl*
879 *Acad Sci U S A* **110**: 18602–18607.

880 Tietjen JR, Zhang DW, Rodríguez-Molina JB, White BE, Akhtar MS, Heidemann M, Li X,
881 Chapman RD, Shokat K, Keles S, et al. 2010. Chemical-genomic dissection of the
882 CTD code. *Nat Struct Mol Biol* **17**: 1154–1161.

883 Tirosh I, Barkai N. 2008. Two strategies for gene regulation by promoter nucleosomes.
884 *Genome Res* **18**: 1084–1091.

885 VanBelzen J, Sakelaris B, Brickner DG, Marcou N, Riecke H, Mangan NM, Brickner JH.
886 2024. Chromatin endogenous cleavage provides a global view of yeast RNA
887 polymerase II transcription kinetics. *eLife* **13**: RP100764.

888 Vermeersch L, Jariani A, Helsen J, Heineike BM, Verstrepen KJ. 2022. Single-Cell RNA
889 Sequencing in YeastYeast Using the 10× Genomics Chromium Device. In *Yeast*
890 *Functional Genomics: Methods and Protocols* (ed. F. Devaux), *Methods in Molecular*
891 *Biology*, pp. 3–20, Springer US, New York, NY https://doi.org/10.1007/978-1-0716-
892 2257-5_1 (Accessed November 14, 2022).

893 Werner-Washburne M, Braun EL, Crawford ME, Peck VM. 1996. Stationary phase in
894 Saccharomyces cerevisiae. *Mol Microbiol* **19**: 1159–1166.

Wery M, Shematorova E, Van Driessche B, Vandenhaute J, Thuriaux P, Van Mullem V. 2004. Members of the SAGA and Mediator complexes are partners of the transcription elongation factor TFIIS. *EMBO J* **23**: 4232–4242.

Wong KH, Jin Y, Struhl K. 2014. TFIIH Phosphorylation of the Pol II CTD Stimulates Mediator Dissociation from the Preinitiation Complex and Promoter Escape. *Mol Cell* **54**: 601–612.

Xi S, Nguyen T, Murray S, Lorenz P, Mellor J. 2024. Size fractionated NET-Seq reveals a conserved architecture of transcription units around yeast genes. *Yeast* **41**: 222–241.

Young CP, Hillyer C, Hokamp K, Fitzpatrick DJ, Konstantinov NK, Welty JS, Ness SA, Werner-Washburne M, Fleming AB, Osley MA. 2017. Distinct histone methylation and transcription profiles are established during the development of cellular quiescence in yeast. *BMC Genomics* **18**: 107.

FIGURE LEGENDS

Figure 1. Transcriptional shutdown during quiescence entry occurs independently of telomere hypercluster formation

A. Timeline of events occurring during quiescence entry. Samples in the nutrient exhaustion kinetics are shown as a function of time after inoculation in rich liquid medium (YPD). All cells following diauxic shift (DS) are sorted through a density gradient (Allen et al., 2006) to recover the highly dense (HD) fraction. For abrupt starvation, yielding Q-like cells, gradient-enriched cells grown for +24h to post-diauxic shift (day1-HD cells) are re-suspended in water for 24h hours.

B. Proportion of nuclei with hyperclusters during quiescence entry compared to spike-in calibrated RNAPII ChIP-seq (Rpb3-FLAG) counts genome-wide. (top) Representative images of Rap1-GFP sampled during quiescence entry. Bar = 1µm. (middle) Rap1-GFP cluster intensities relative to total nuclear signal classified according to the number of clusters found per nucleus. Hyperclusters, shown in blue, are defined as clusters with a relative intensity over four-fold higher than the average cluster in Log phase. Pie charts represent the proportion of nuclei with a hypercluster. (bottom) Rpb3-FLAG spike-in calibrated IP counts averaged over 1kb bins genome-wide.

C. Comparison of telomere hyperclustering and Pol II (Rpb3-FLAG) binding in quiescence (6dHD, Q). (Left) Representative images of Rap1-GFP in WT and *sir3*Δ samples in quiescent cells. Small cells, with a Feret's diameter < 4.5 µm are marked with an asterisk (*) in transmitted light images. Bar = 1µm. (Right) Rpb3-FLAG counts over genes normalized by gene size in WT vs *sir3*Δ samples.

Figure 2. The dismantling of telomere hyperclusters during return to growth follows but is independent of transcriptional activation.

A. Telomere hypercluster dismantling upon quiescence exit. Representative images of Rap1-GFP sampled during quiescence release. Brightness for all Rap1-GFP images is set at 1600 maximum.

B. Telomere hypercluster dismantling in rich medium (YPD) after shifting cells grown at 25ºC to restrictive temperature (37ºC, methods) to inactivate RNAPII (*rpb1-1*) or not (WT) for RNAPII transcription: representative Rap1-GFP images after 15 or 30 min of refeeding of stationary phase cells. Brightness for all Rap1-GFP images is set at 1600 maximum.

Figure 3. Transcriptional output is scant, but homogeneous, in the quiescent population

A. Representative genome browser views of genes classified according to binarized Rpb3-FLAG binding and recently synthesized transcripts detection within the coding region. Thresholds are set at 50 average counts for Rpb3-FLAG and 1 average count for 4tU-seq (see Supplemental Fig. 3 C, D, F). *This study. **Rpb1 CTD-Ser2P and recently synthesized transcripts mappings are from the Tsukiyama laboratory (Swygert et al., 2019, Cucinotta et al., 2021).

B. UMAP representation of cells in the quiescent population assessed by scRNA-seq. Colour scale represents the percentage of the transcriptome per cell for the sum of class I genes.

C. (left) List of top 7 class I genes, representing 18.8% of the transcriptome of the average cell. (right) Genome browser view of *GRE1*, detected in >99% of 6d-HD (Q) cells, during early respiration (Day 1 HD) and in two types of quiescence induction (abrupt starvation from post-diauxic shift, Q-like; nutrient exhaustion after 6 days, Q). *This study. **Rpb1 CTD-Ser2P and recently synthesized transcripts mappings are from the Tsukiyama laboratory (Swygert et al., 2019, Cucinotta et al., 2021).
Intergenic accumulation of Rpb3-FLAG upstream of genes in Q samples (6d-HD) is highlighted in gray to allow comparison across conditions.

Figure 4. RNAPII re-distributes to a subset of promoter-bearing intergenes when cells enter quiescence

A. Rpb3-FLAG spike-in calibrated signal piled-up at the center of intergenes classified based on the orientation of surrounding coding annotations. Rows are sorted based on intergene size.

B. Mapping of RNAPII (Rpb1 C-terminal domain, Rpb1 CTD; Rpb1 CTD Serine 2 phosphorylation, Rpb1 CTD-Ser2P; Rpb1 CTD Serine 5 phosphorylation, Rpb1 CTD

Ser5P) and RNAPI (Rpa135-FLAG) epitopes in and around the RNAPII (Rpb3-FLAG) quiescent peak at the divergent intergene between *DCP2* and *MLS1* (class III genes). (*Top*) Genome browser view of spike-in calibrated Rpb3-FLAG (this study), Rpb1 CTD Serine 2 phosphorylation (Rpb1 CTD-Ser2P, Swygert et al., 2019) and recently synthesized transcripts (4tU-seq, both strands merged, Cucinotta et al., 2021). (*Bottom*) ChIP-qPCR IP/INPUT signal normalized to an intergenic region in ChrI (methods). Antibodies used are written in parentheses.

C. Average profile plot of ChIP-seq or ChIP-array mappings (*z*-scores) of various nuclear proteins in exponential growth (Log) and quiescent (Q 6d-HD) cells: RNAPII (Rpb3-FLAG, this study), TFIIB (Sua7 in Log, Jeronimo et al., 2014; Sua7 in quiescent (6d-HD) cells, Cucinotta et al., 2021) and Sir3 (Guidi et al., 2015). Signals are centered at the summits of RNAPII (Rpb3-FLAG) strongest peaks in quiescence (MACS2 signal Value > 2.4), falling in promoter-bearing intergenes, or at random locations in promoter-bearing intergenes without RNAPII peak overlap. (*Right*) Coverage tracks of samples shown in left panel at *DCP2/MLS1* intergene.

D. Pie charts depicting the proportion of genes bearing an RNAPII summit in the vicinity of their promoter, stratified by transcription status in quiescence, as described in Fig. 3A. (p-values for hypergeometric test: I**, 2.23×10^{-03}; III***, 1.23×10^{-43})

Figure 5. Quiescence-specific intergenic RNAPII accumulates at non-canonical binding sites in promoters

A. RNAPII distribution over coding sequences at 137 RP (Ribosomal Protein), 938 STM (SAGA, Mediator or TUP- bound) and 1783 TFO (TF organization lacking STM cofactors but bound by insulators) genes (Rossi et al. 2021). Rpb3-FLAG signal (*z*-score) is re-scaled over TSS-TES.

B. Distribution of summits falling in promoter-bearing intergenes relative to transcription start sites (TSS). TSS positions are corrected using CRAC-seq from cycling cells (Candelli et al. 2018). Locations of mapped upstream activated sequences (Schofield and Hahn 2023) are shown as dark red lines.

C. Transcription factor binding sites (TFBS from JASPAR 2022 fungi database (Castro-Mondragon et al. 2022)) found in the vicinity (100 bp) of strongest RNAPII intergenic summits, with a fold enrichment over control > 3 (SEA, MEME suite (Bailey and Grant 2021)).

D. Clustering of Rpb3-FLAG at Q summits +/- 1kb (Top) Average profile plot of RNAPII ChIP-seq (Rpb3-FLAG, this study). Signals are centered at the summits of RNAPII (Rpb3-FLAG) in quiescence falling in promoter-bearing intergenes. Summits are clustered (*k*-means) into three groups: 437 summits with signal present throughout the kinetics of Q entry, 601 summits with signal localy depleted during growth phase and 404 summits appearing *de novo* in the later stages of quiescence entry. (bottom) Snapshots of Rpb3-FLAG mapping (*this study) in fermentation (Log), respiration (post-diauxie, day1 HD; day 2 HD) or quiescence induced by abrupt starvation (Q-like) or nutrient exhaustion (Q, 6d HD). Typical examples are shown below each group. Dotted lines indicate the position of the peak summit for each intergene and grey boxes indicate the region over which the signal was clustered.

Figure 6. Upstream RNAPII predicts strength of transcriptional re-start upon release

A. *k*-means clustering of recently synthesized transcripts data (**Cucinotta et al., 2021) over TSS-TES. Shown are the number of genes per cluster. Pie charts show the proportion of genes per cluster bearing an upstream RNAPII summit (black). Outer ring shows the proportion of ribosomal protein genes (blue). *** gene clusters significantly enriched in RNAPII at promoter (hypergeometric test, R-I, 1.14×10^{-4}; R-II, 2.32×10^{-27}; R-III, 3.75×10^{-39}; R-IV, ns)

B. Heatmap of RNAPII enrichment at promoter per decile of expression in single cell RNA transcriptomes performed 30 min after release in media containing different carbon sources. RNAPII enrichment at promoter was estimated by a hypergeometric test on the proportion of genes with a Rpb3-FLAG peak summit falling in the upstream intergene (p-values shown in S6F). Deciles of expression are based on the number of cells expressing the gene per sample (cells released on media containing either glucose (2%) or lactate and ethanol (0.5 %, 2%) as carbon source). Pie charts represent the proportion of genes with (black) or without (grey) a summit in their promoter amongst the 10% most frequently expressed genes in either condition. Outer ring shows the proportion of ribosomal protein genes (blue), as in panel A. *** indicate significant enrichment in RNAPII summits at promoter.

Figure 1

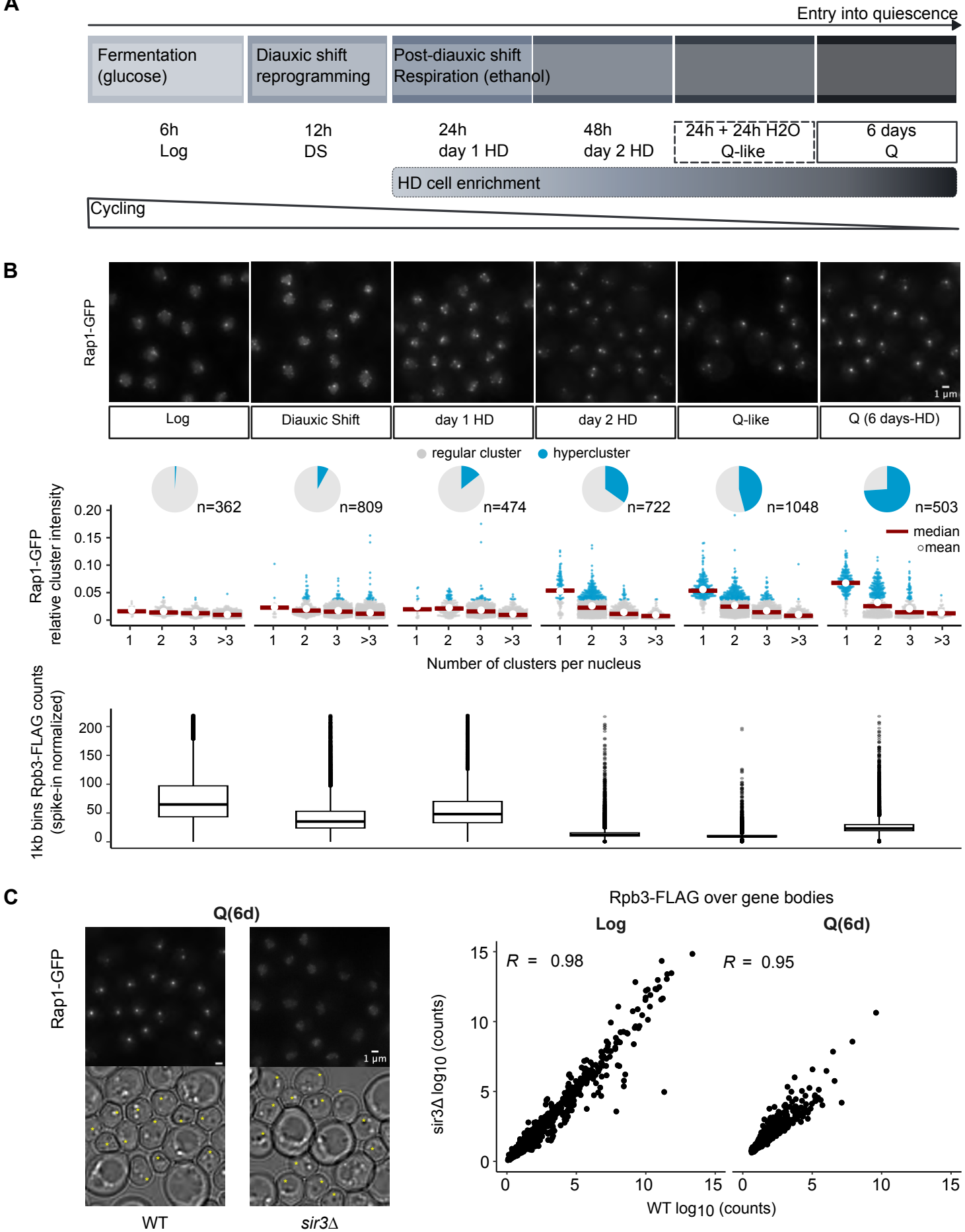

Figure 2

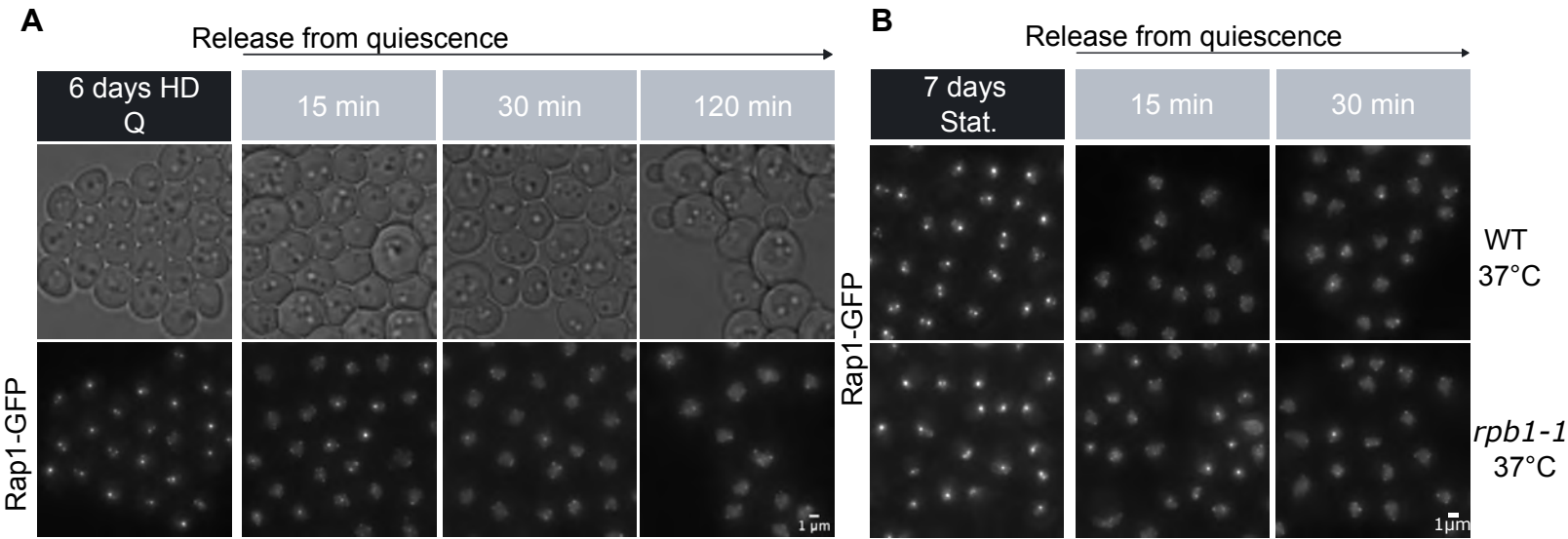
A
Release from quiescence
6 days HD Q
15 min
30 min
120 min
Rap1-GFP
1 µm
B
Release from quiescence
7 days Stat.
15 min
30 min
Rap1-GFP
WT 37°C
rpb1-1 37°C
1µm

Figure 3

A

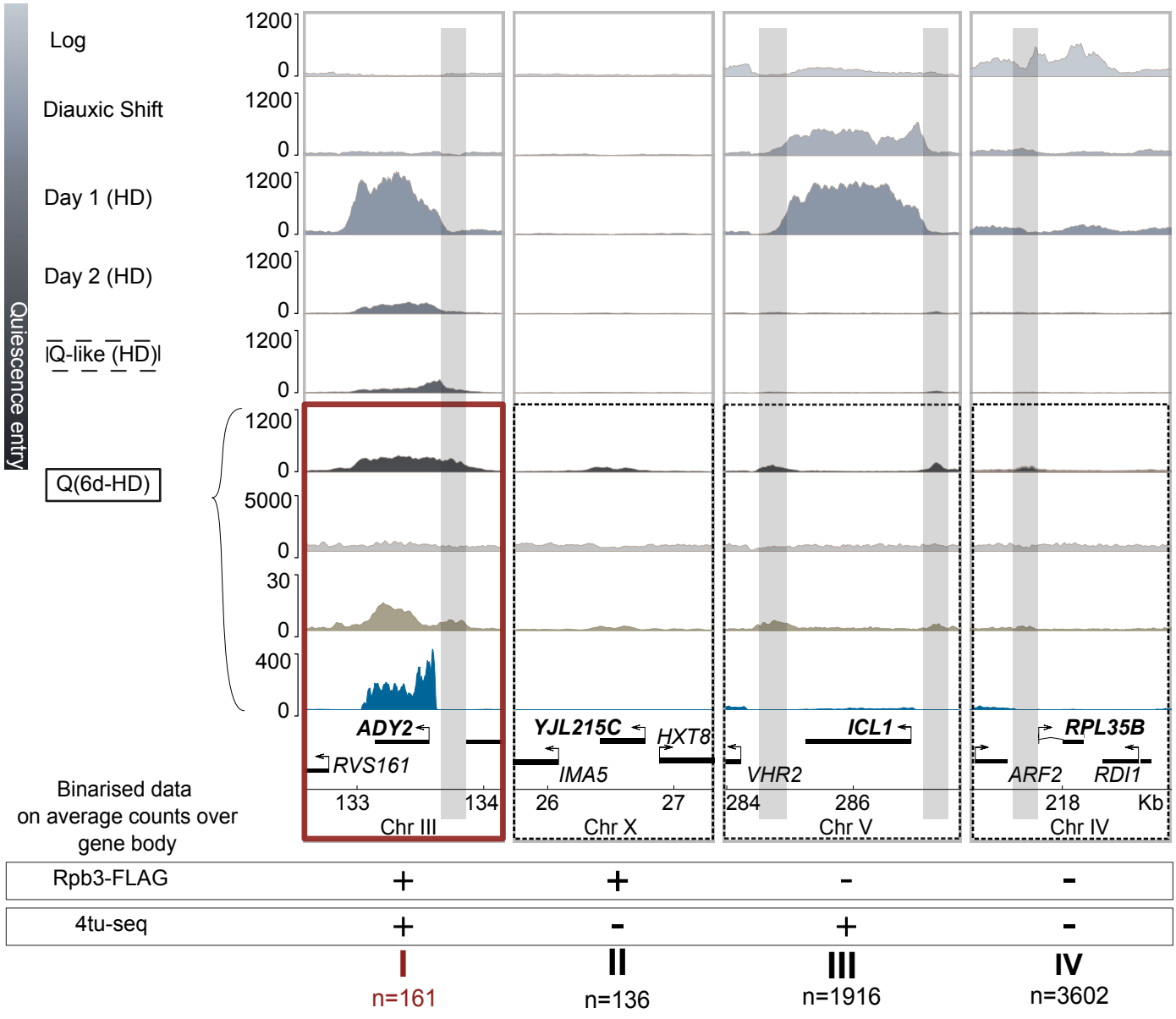

Binarised data on average counts over gene body

	I	II	III	IV
Rpb3-FLAG	+	+	-	-
4tu-seq	+	-	+	-
	n=161	n=136	n=1916	n=3602

B

6 days - HD **(Q) population**

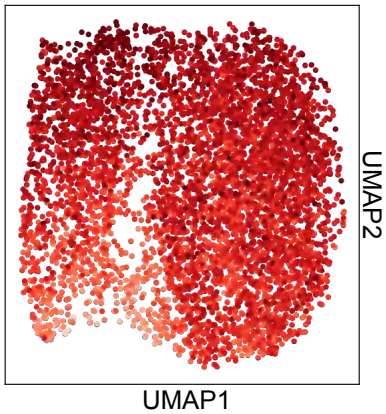

% of transcriptome of class I genes

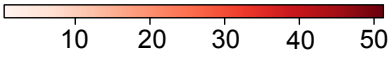

C

top 7 class I genes
detected in > 80% of cells
proportion of transcriptome > 1%

systematic name	standard name	name description SGD
YPL223C	***GRE1***	*Genes de Respuesta a Estrés* 1 (spanish for Stress Responsive Genes)
YMR175W	***SIP18***	Salt Induced Protein 1
YLR327C	***TMA10***	Translation Machinery Associated 10
YKL065W-A		
YOL052C-A	***DDR2***	DNA Damage Response 2
YER084W		
YGR236C	***SPG1***	Stationary Phase Genes 1

GRE1
detected in 99% of 6d-HD (**Q**) cells

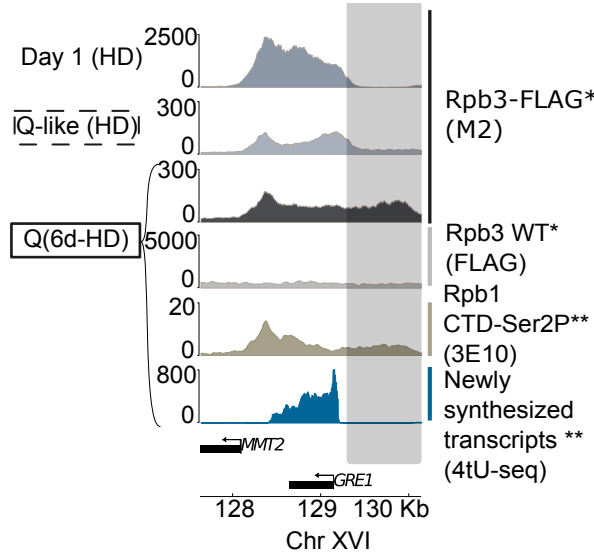

Figure 4

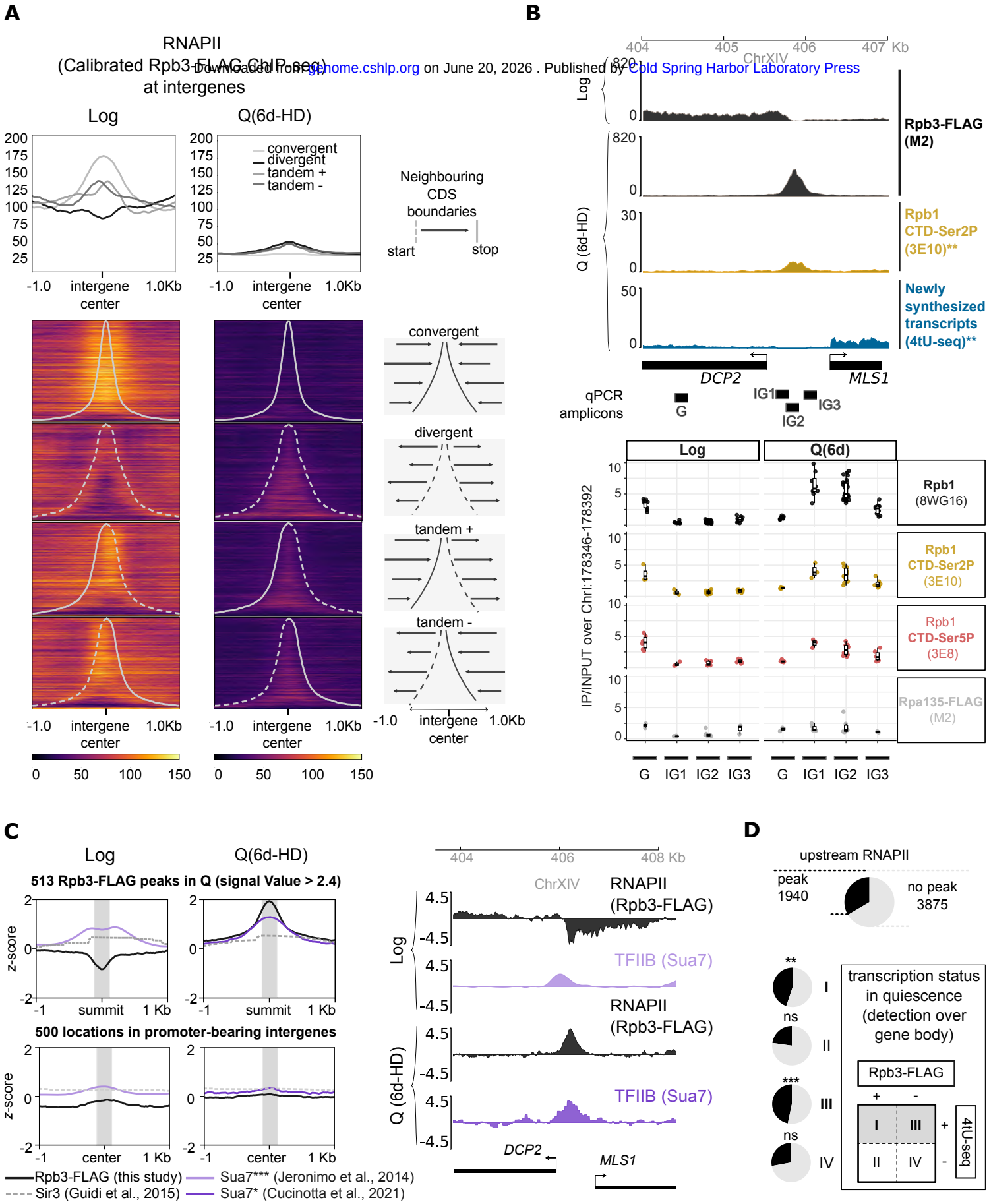

Figure 5

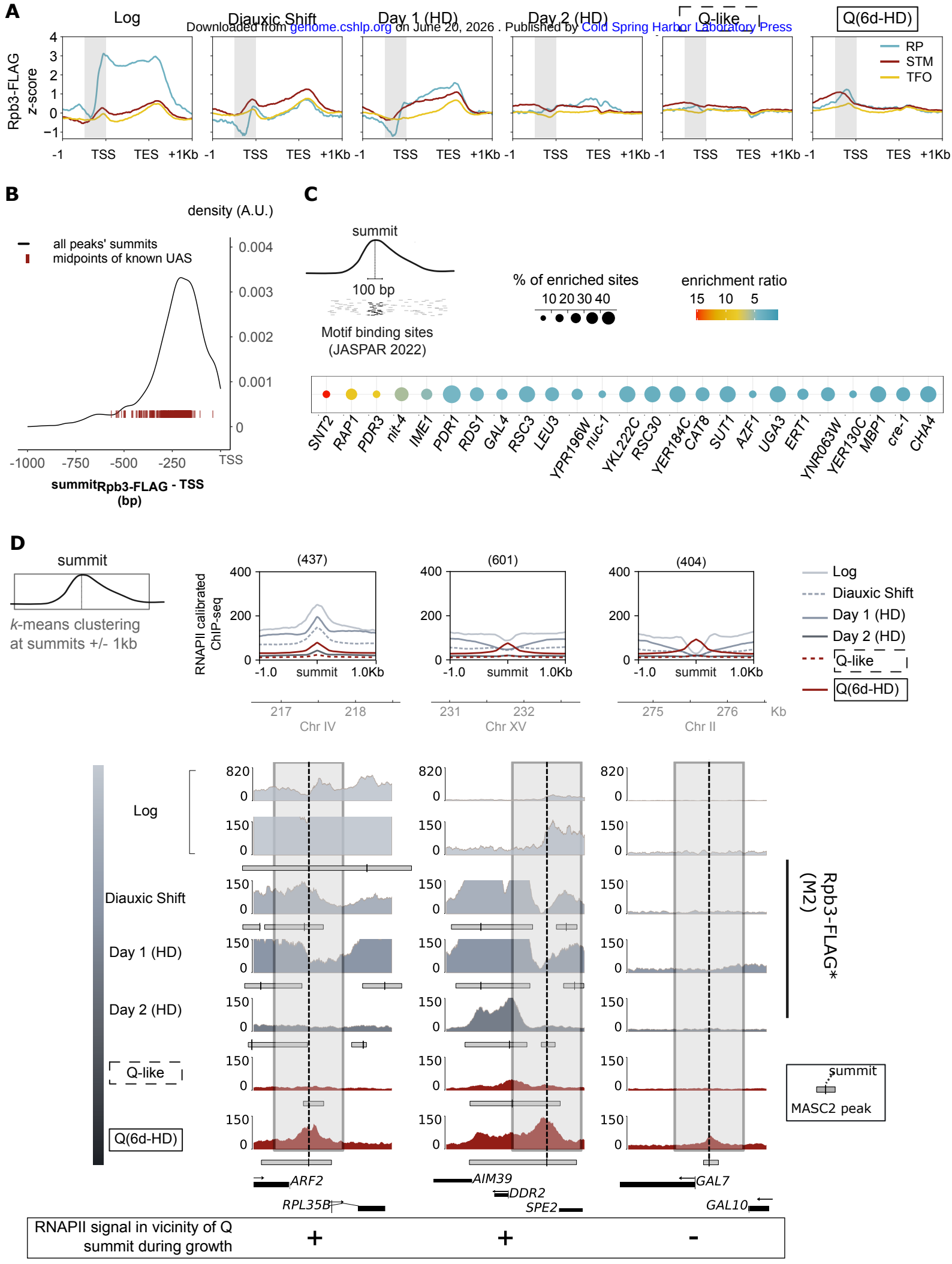

Figure 6

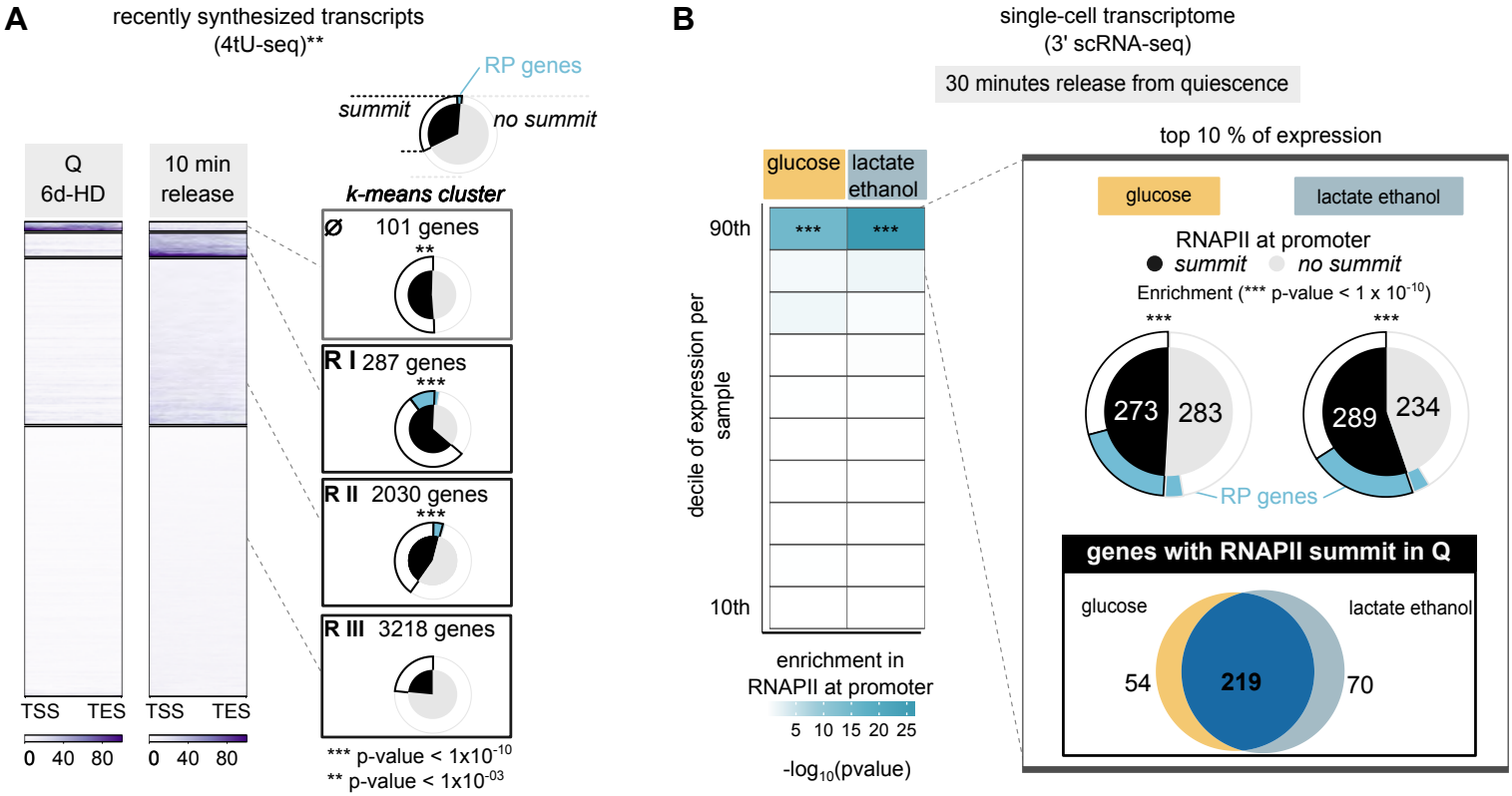
A
recently synthesized transcripts
(4tU-seq)**
RP genes
summit
no summit
Q
6d-HD
10 min
release
k-means cluster
Ø 101 genes
**
R I 287 genes
***
R II 2030 genes
***
R III 3218 genes
TSS TES
TSS TES
0 40 80
0 40 80
*** p-value < 1x10-10
** p-value < 1x10-03
B
single-cell transcriptome
(3' scRNA-seq)
30 minutes release from quiescence
glucose
lactate ethanol
90th
10th
decile of expression per sample
***
***
enrichment in RNAPII at promoter
5 10 15 20 25
-log10(pvalue)
top 10 % of expression
glucose
lactate ethanol
RNAPII at promoter
summit
no summit
Enrichment (*** p-value < 1 x 10-10)
***
***
273
283
289
234
RP genes
genes with RNAPII summit in Q
glucose
lactate ethanol
54
219
70